The effect of step height on the performance of three-dimensional ac electro-osmotic microfluidic pumps

John Paul Urbanski [a,b], Jeremy A. Levitan [b,c], Damian N. Burch [c], Todd Thorsen [a,b], Martin Z. Bazant [b,c,*]

[a] *Department of Mechanical Engineering, Massachusetts Institute of Technology, Cambridge, MA 02139, USA*
[b] *MIT Institute for Soldier Nanotechnologies, Cambridge, MA 02139, USA*
[c] *Department of Mathematics, Massachusetts Institute of Technology, Cambridge, MA 02139, USA*

Abstract

Recent numerical and experimental studies have investigated the increase in efficiency of microfluidic ac electro-osmotic pumps by introducing nonplanar geometries with raised steps on the electrodes. In this study, we analyze the effect of the step height on ac electro-osmotic pump performance. AC electro-osmotic pumps with three-dimensional electroplated steps are fabricated on glass substrates and pumping velocities of low ionic strength electrolyte solutions are measured systematically using a custom microfluidic device. Numerical simulations predict an improvement in pump performance with increasing step height, at a given frequency and voltage, up to an optimal step height, which qualitatively matches the trend observed in experiment. For a broad range of step heights near the optimum, the observed flow is much faster than with existing planar pumps (at the same voltage and minimum feature size) and in the theoretically predicted direction of the "fluid conveyor belt" mechanism. For small step heights, the experiments also exhibit significant flow reversal at the optimal frequency, which cannot be explained by the theory, although the simulations predict weak flow reversal at higher frequencies due to incomplete charging. These results provide insight to an important parameter for the design of nonplanar electro-osmotic pumps and clues to improve the fundamental theory of ACEO.
© 2007 Elsevier Inc. All rights reserved.

Keywords: Electrokinetics; Electro-osmosis; Microfabrication; Microfluidics; Pump

1. Introduction

Traditional pressure-driven flows in microfluidics do not scale well with miniaturization due to large viscous stresses, so several alternative pumping techniques have been explored [1,2]. In particular, fluids may be transported using electrical fields, which do not involve moving parts and are readily integrated within microchannels using standard microfabrication approaches. In conventional capillary electro-osmosis (EO), a liquid electrolyte effectively slips past solid surfaces in a plug-shaped profile due to an applied electric field, which circumvents the penalty of miniaturization presented by standard hydraulic resistance. EO driven flows are widely used, although there are several potential limitations, such as strong sensitivity to the surface and solution chemistry (which can cause flow reduction or reversal), the need to sustain DC current through Faradaic reactions at the electrodes (resulting in typically unwanted effects, such as solution contamination, concentration gradients, electrode degradation, and bubble formation from hydrolysis), and the possibility of electrokinetic instability in the presence of concentration gradients (which can enhance mixing but also hinder pumping and local fluidic control) [3]. Voltages in the kiloVolt range are typically required to drive EO flows, which exacerbates these effects and dictates that EO-based microfluidic analysis systems be operated with independent, external power supplies.

An alternative approach to pumping fluid through microchannels is nonlinear AC electro-osmosis (ACEO). In the first experimental study by Ramos et al., sustainable fluid circulation was generated using low AC voltages applied between

* Corresponding author.
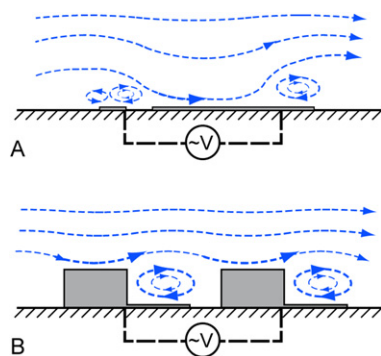 *E-mail address:* bazant@mit.edu (M.Z. Bazant).

Fig. 1. Time-averaged fluid streamlines resulting from the application of an alternating voltage to two different ACEO pumps. (A) Planar asymmetry results in directional pumping through a biased competition between opposing slip developed on the electrode pairs. (B) The fluid conveyor belt principle is realized using nonplanar electrodes to naturally exploit the counter-directional vortices. Fluid flow is increased for the same applied voltage using this efficient approach. The effect on pump performance as a function of the electrode step height remains an open design problem.

two electrodes on an insulating substrate [4], although due to symmetry, no net pumping was created. Ajdari postulated that the ACEO mechanism could be used to generate directional pumping over the interdigitated electrode pairs by breaking symmetry in a variety of ways, either by modifying surface capacitances or by gently modulating the surface heights of the electrodes [5]. Alternatively, it has been experimentally demonstrated that directional pumping can be achieved by modulating the distances between, and widths of, interdigitated planar electrode pairs [6], which has become the standard realization of ACEO pumps in microfluidics [7–9] and the focus of several theoretical investigations [10–12]. Some recent research has also considered pumping by traveling wave voltages in symmetric arrays, but still with planar electrodes [13,14].

It was only recently realized that modulating the surface height, beyond the regime of small perturbations analyzed by Ajdari, is a remarkably effective form of symmetry breaking to achieve fast pumping over an electrode array applying an AC voltage. In particular, Bazant and Ben suggested using nonplanar "3D" electrodes with asymmetric raised steps to create a "fluid conveyor belt" (FCB), and they predicted enhanced flow rates by more than an order of magnitude over existing planar ACEO pumps (for the same minimum feature size and operating voltage) using the standard low-voltage theory [15]. Nonplanar electrodes had never been investigated in ACEO pumps prior to that work, so we performed our first experiments to test the qualitative predictions of the theory for a particular nonplanar design [16], compared to the state-of-the-art in planar ACEO pumps [6,7,9]. Dramatically increased flow rates were clearly observed, but our experiments also revealed several features not captured by the theory, such as a double-peaked frequency dependence and high-frequency flow reversal at large voltages [16].

In spite of the complicated behavior of 3D ACEO pumps in experiments, the basic FCB mechanism for greatly enhanced flow rates is very simple, as illustrated in Fig. 1. Rather than biasing the competition between reverse slipping surfaces on nearly planar electrodes, as originally suggested by Ajdari [5],

substantially raising the portion of each electrode surface with electro-osmotic slip in the desired pumping direction, and recessing the portion with reverse slip, turns competition into cooperation. The reverse flows recirculate in recessed vortices to form "rollers" which enhance the nearly uniform pumping flow generated by the raised surfaces, as in a conveyor belt.

In this paper, we continue building on the recent discovery of 3D ACEO by exploring the dependence of the flow rate on the electrode height. Typically, planar ACEO devices are characterized by two electrode widths, two electrode separations, and a microchannel height [10]. 3D ACEO introduces additional geometrical parameters to consider, including the height, width and location of three-dimensional steps on the base electrodes. This new, third dimension is the subject of this present study where the physical height of the steps are varied as means to improve pumping performance.

Such three-dimensional steps are readily fabricated on ACEO devices using a combination of photolithography and electroplating. In microfabrication of ACEO pumps, however, varying the width of the steps is not straightforward as a new photomask for the patterning of each electroplating pattern is required. Bazant and Ben [15] suggested that the optimal width of an electrode step is approximately one-half the width of the planar electrode, with the step aligned to the trailing edge of the base, although they did not perform a systematic optimization of the geometry. A recent optimization study by Olesen [11] varying this and other parameters using the same electrokinetic model, however, did not obtain substantially enhanced flow rates over the original examples of Bazant and Ben. Therefore, in this work, we choose to fix the step width at one half of the electrode width, and we focus on the effect of varying the step height, which is the most important and novel parameter in 3D ACEO pump designs.

To implement the nonplanar geometries, an array of interdigitated planar electrodes with symmetric widths and separations is first fabricated on an insulating substrate. Without the addition of steps, no net pumping can be generated due to geometrical symmetry. Several devices with a range of step heights are created by controlling the electroplating process, which vary in height up to one-half of the electrode width. Each different height of electrokinetic pump may exhibit fluid pumping behavior in response to various applied voltages and AC frequencies.

The expected pumping performance based on the height dependence is first parametrically examined with numerical simulation of the electrokinetics problem, using the standard low-voltage model described in Refs. [10,11,15,17]. Next, the experimental measurements of 3D ACEO pumping velocities are systematically performed using a custom designed microfluidic device and particle image velocimetry. Above a threshold step height needed to create the FCB mechanism, a rich velocity-frequency response occurs around an optimal step height for maximum pumping, while the flow decays at larger step heights. Below the threshold height, a new regime of weaker flow in the reverse direction is observed. These results suggests the existence of an optimal step height for a given electrode width.

2. Experimental methods

2.1. Pump fabrication

The electrokinetic pumps are fabricated using a series of photo-patterning, etching, and electroplating steps. A 50 nm adhesion layer of chrome, followed by a 50 nm layer of gold is deposited by e-beam evaporation onto 4-inch borosilicate glass wafers which have been previously cleaned in a piranha solution (1:3 solution of hydrogen peroxide and sulfuric acid) for 20 min and roughened in a barrel asher for 2 min. The planar electrode structures are created by etching patterns with gold and chrome etchants, defined using standard positive resist photolithography (OCG 825) and a high resolution chrome mask. Three-dimensional structures are created using a secondary photolithography and electroplating process. A second mask is aligned to base features, and a thick photoresist (10 μm, AZ 4620) is patterned for electroplating. Steps are electroplated to a desired height using gold solution (Orotemp 24C, Technic, Inc.) and the residual photoresist is stripped using acetone and isopropanol. The plating height is varied by adjusting the electroplating current and time. Individual rectangular devices are die-sawed, and, prior to testing, bare copper leads are attached using conductive silver epoxy. The resulting heights of the three-dimensional structures are measured using a white light interferometer (Zygo Corp.).

2.2. Microfluidic devices

A microfluidic chip is designed to systematically study the performance of the various pump designs, following a similar methodology described previously by Studer et al. [9]. The devices are comprised of an assembly of the base glass substrate containing patterned electrodes, capped with a polydimethylsiloxane (PDMS) microfluidic device [18]. On chip valves isolate fluid flow due to electrokinetic pumping from external pressure perturbations and are controlled using off chip pressure regulators. The testing loops have a circumference of 20 mm, and pump lengths are 5 mm.

Microfluidic devices in this study are created using multilayer soft lithography (MSL) [18]. The PDMS device is designed to allow channels of rectangular cross section to be used in the pumping loop. Previous studies using an enclosed loop [9] relied on "push-down" MSL valves, which necessitate rounded flow channels. Rounded channels complicate fluid flow profiles, place a limit on the height of fluid channels which may be tested, and are not adequate for accommodating tall rectangular electroplated structures. The present design improves on the previous approach by utilizing internal interconnects between rectangular and rounded channels on two device layers, created by punching small holes in the thin PDMS membrane. In this manner, rectangular channels on the base layer may be used to create "push-up" valves [19] to control fluid flow into the loop, and pressurized fluids may also be routed from rounded channels in and out of rectangular channels below. Rectangular channels of arbitrary height may also be tested

within such loops in order to study the effects of electric field confinement on pumping [10].

The injection layer mold is fabricated using a positive resist (AZ 4620, Clariant) on a silicon wafer, which is reflowed after development to create molds of rounded cross section. Flow molds are created using a negative photoresist (SU-8 2050, Microchem) resulting in channels of rectangular cross section. A two layer microfluidic device is created using PDMS (Sylgard 184, Dow Corning). The top layer is cast using the injection mold, and aligned over a thin layer of partially cured PDMS which has been spun coat on the flow mold. After curing, devices are peeled from the molds and fluidic connections are punched with a flat luer stub adapter (BD Biosciences). Interconnects between the top and bottom fluid layers are created by small cuts with a scalpel. Injection and flow channels are 10 μm and 80 μm tall respectively, and both are 100 μm wide. Uniformity of all molds is ensured using a white light interferometer, and heights are found to vary by no more than approximately 1 μm over all channels.

A plasma treatment is used to seal the ACEO substrates and PDMS caps, which are aligned and bonded under a microscope such that the 100 μm wide microchannels of rectangular cross section completely enclose the 80 μm wide plated pump structures. Complimentary grids on both the glass substrate and PDMS cap facilitate manual alignment within this tolerance.

A representative microfabricated pump with electroplated steps and the microfluidic device is pictured in Fig. 2. Fig. 2A presents a scanning electron micrograph of the interdigitated fingers of a characteristic pump of the present study. Fig. 2B shows a photo micrograph of the lower half of the microfluidic experimental setup, including fluid control inputs and valve channels, and the gold ACEO pump.

2.3. Measurement procedure

Fluid purging and metering operations are software controlled using micro-solenoids connected to the integrated MSL valves [18]. Pressurized reservoirs of operating fluid (dilute potassium chloride), and a solution containing 1:250 tracers:water (v/v) are connected to the microfluidic device via tygon tubing. One input channel is used to load a solution of operating fluid in the loop, and the second input is used to inject flow markers (1.0 μm diameter fluorescent tracers, 505EX/515EM, Molecular Probes) in the corner of the pumping loop away from the electrodes to prevent interference due to electrophoresis or contamination of the pumps with particles [9]. In the present study, dilute KCl was arbitrarily chosen as a working fluid to focus systematically on the effect of three-dimensional geometry. It should be noted that additional precautions may be required to control the presence of dissolved ions from other sources in our fluid if effects of solution chemistry were of primary interest.

A signal generator (Agilent 3320A) is used to operate the ACEO pumps at various AC frequencies (0.5–10 kHz), at 3 V peak-to-peak (Vpp). Movies of the fluid far from the electrodes are recorded using a camera (Sony XCD-V50 B/W, 640 × 480 pixels) under an inverted fluorescent microscope
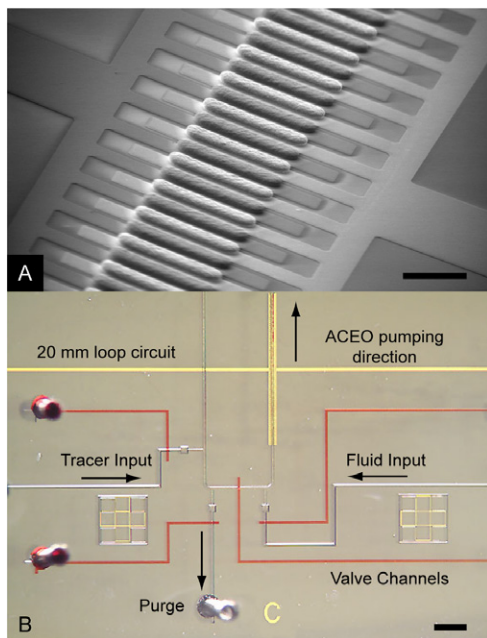
Fig. 2. (A) Scanning electron microscope image of a 3D ACEO pump comprised of interdigitated gold electrodes patterned on an insulating substrate. The scale bar indicates 100 μm. (B) The microfluidic device containing an integrated pumping loop with rectangular channels allows for repeatable characterization of different 3D ACEO pumps. When an alternating voltage is applied to the electrodes, the fluid is pumped in the counter clockwise direction within the closed circuit. Fresh operating fluid is loaded to the loop over the pumps, and tracer particles are input to the bottom left hand corner before every velocity measurement. The scale bar indicates 1 mm.

with a 20× objective at each driving frequency in a similar manner for all pumps. The focal point of the microscope is set to the centerline of the microchannel to record the fastest moving particles. In order to achieve repeatable measurements and avoid any history effects on pumping, newly assembled devices are preconditioned for 60 min by pumping on fluid which does not contain beads. The pumping loop also is purged with fresh operating fluid prior to each measurement. Particle movies are analyzed using an open source particle image velocimetry code (URAPIV) through a MATLAB routine, which has been found to provide velocity measurements with less than 5% absolute error in calibration studies.

3. Numerical methods

3.1. Theory

AC electro-osmosis is a complicated phenomenon of electrochemical hydrodynamics, particularly in three-dimensional electrode geometries. As such, we follow prior authors in making a number of simplifications to allow for efficient numerical simulation. We assume that the electrodes are sufficiently wide in the transverse direction for the problem to be effectively two-dimensional, and that the electrode array is sufficiently long for us to simulate a single electrode pair with periodic boundary conditions and ignore edge effects at the ends of the array. More importantly, we adopt the simple mathematical model used in previous simulations of ACEO pumps [4,5,8,10,12–15,20]

and other phenomena of induced-charge electro-osmosis [17, 21,22], which can only be justified for small voltages [22], $V \ll kT/e = 25$ mV. Unfortunately, ACEO experiments always involve much larger voltages [4,6–9,12,16] for which the theory becomes much more complicated and is not yet fully developed [15,23,24]. Nevertheless, the standard model has succeeded in capturing at least qualitative features of many experiments, so we test it here as a reasonable first approximation.

The standard model has been described in many prior papers, so here we simply summarize the equations and basic assumptions. The first assumption is that the double layers are thin enough to be treated as mathematical boundary layers surrounding a quasi-neutral bulk electrolyte, even during charging dynamics [25]. During nonlinear electrochemical relaxation in response to a large applied voltage, the bulk solution can develop concentration gradients due to salt adsorption and tangential conduction by the double layers [25,26], but such effects are model specific and have only begun to be considered in simulations of ACEO [10,11]. Below a threshold voltage (a few times kT/e [23–25], however, it can be assumed that the bulk concentration (and conductivity) remain nearly uniform. In this limit, the bulk electrostatic potential satisfies Laplace's equation (Ohm's law), and the fluid velocity plays no role in the electrochemical dynamics, even with a large Peclet number. Neglecting Faradaic reactions, the double layer on each electrode acts like a capacitor with a constant capacitance in the linear regime of small voltages ($<kT/e$) [4,5,20] or a nonlinear differential capacitance at larger voltages, which depends on the specific model of the double layer [10,23,24]. The nonelectrode surfaces are assumed to be inert and nonpolarizable.

Typical flow velocities in ACEO experiments are on the order of a few millimeters per second. The fluid problem is therefore well into the incompressible, viscous flow regime, and we may employ the time-dependent Stokes equation. The final crucial assumption is that the induced-charge electro-osmotic slip velocity (outside the double layers) on the electrodes is given by the Helmholtz–Smoluchowski formula, although this should in principle be modified at large voltages. Since the nonelectrode surfaces are assumed to be nonpolarizable, they can only permit linear fixed-charge electro-osmotic flows, which vanish upon time averaging, yielding effectively a no-slip condition.

For small voltages ($<kT/e$), the complete system of equations and boundary conditions is linear, so we follow Gonzalez et al. [20] (and our group [17]) in focusing on the steady sinusoidal response to a single-frequency AC voltage. The electrostatic potential, $\phi(x, y, t) = \text{Re}[\Phi(x, y)e^{i\omega t}]$, is expressed in terms of a time-independent complex-valued amplitude $\Phi(x, y)$, which satisfies Laplace's equation

$$\nabla^2 \Phi = 0 \tag{1}$$

with the "RC" boundary condition at the electrode surfaces

$$\hat{n} \cdot \nabla \Phi = \frac{i\omega \varepsilon_w \Lambda}{\sigma \lambda_D}(\Phi \mp V_{peak}) \tag{2}$$

and an insulating boundary condition at the nonelectrode surfaces

$$\hat{n} \cdot \nabla \Phi = 0. \tag{3}$$

Here ε_w is the permittivity of the solution, σ is the electrical conductivity of the solution, λ_D is the Debye length, V_{peak} is the amplitude of V_{pp} applied, and Λ is the fraction of the total voltage across the double layer which is dropped across the diffuse layer (in the linear model). The latter is usually written as $\Lambda = (1 + \delta)^{-1}$, where δ is the ratio of the diffuse-layer capacitance to the compact-layer capacitance [5,17,25]. Note that

$$\tau_c = \frac{\varepsilon_w L \Lambda}{\sigma \lambda_D} = \frac{\lambda_D L \Lambda}{D} \tag{4}$$

is the natural "RC" time scale for charging of the double layers, where L is the geometrical length scale (usually the minimum feature size) and D is the typical ionic diffusivity [25]. The time-averaged fluid velocity is governed by the incompressible Stokes equations:

$$\nabla \cdot u = 0, \tag{5}$$
$$\nabla p = \eta \nabla^2 u \tag{6}$$

with no-slip conditions at nonelectrode surfaces and the Helmholtz–Smoluchowski formula in the following form at the electrodes:

$$u_{||} = \frac{\varepsilon_w \Lambda}{2\eta} \big(\mathrm{Re}[\pm V_{peak} - \Phi] \mathrm{Re}[\partial \Phi / \partial x]$$
$$+ \mathrm{Im}[\pm V_{peak} - \Phi] \mathrm{Im}[\partial \Phi / \partial x] \big), \tag{7}$$
$$u_\perp = 0. \tag{8}$$

Here u is the time-averaged velocity field ($u_{||}$ parallel and $u_\perp$ perpendicular to the electrode surface), p is the time-averaged pressure field, η is the dynamic viscosity of the solution, and x is the coordinate along the electrodes.

3.2. Simulation

Simulations are completed using COMSOL Multiphysics 3.2b (COMSOL, Burlington, MA), a commercial program for performing electrical and hydrodynamic simulations using finite element methods, following methodologies previously described [15,17]. Each simulation uses an automatically generated, triangular mesh and quadratic Lagrangian shape functions. The mesh sizes are dependent on the exact geometry being studied; for the simulations for which results are presented herein, a typical mesh has approximately 35,000 elements and 1000 boundary elements.

Model dimensions and nomenclature are illustrated schematically in Fig. 3. The geometry may be specified arbitrarily, and is parametrically changed inside MATLAB scripts. Once the geometry is fixed, the mesh is automatically generated. The electrical problem is then solved and used as an input for solving the fluid system. Our typical measure for pumping speed is the average value of the velocity (in the x-direction) along the periodic boundary of the system.

It should be noted that even though the electrodes are relatively short, their sides (i.e., the step risers) must still be treated as electrode surfaces, i.e., we must employ the double-layer capacitance model and the Helmholtz–Smoluchowski slip formula on all sides of each electrode that are in contact with the
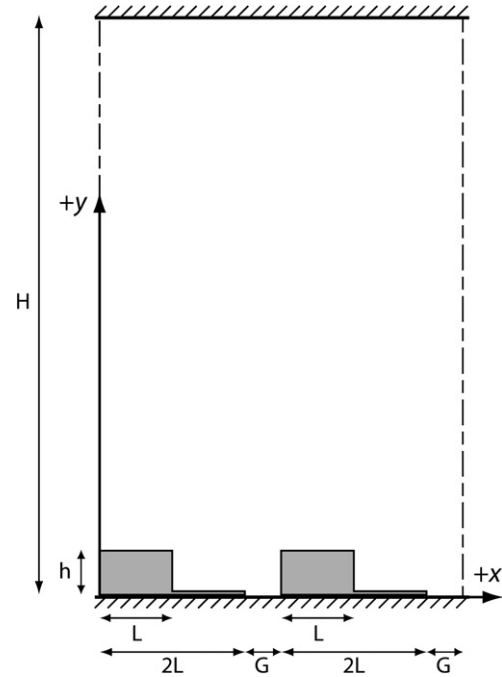

Fig. 3. Schematic of the ACEO geometry used in the numerical model, with one complementary electrode pair located on an insulating substrate. Expected fluid pumping due to the FCB mechanism is in the positive x-direction. The values of L, G, and H in the present study are 10, 5, and 80 μm, respectively. Periodic boundary conditions are imposed in the direction normal to the fluid flow, and no slip boundary conditions are imposed on the nonelectrode surfaces. The heights of ACEO steps, h, range from 0 to 10 μm.

solution. Ignoring this requirement can lead to significant discrepancies in the results.

4. Results and discussion

4.1. Numerical and theoretical results

It is clear from Eq. (2) that the appropriate nondimensional frequency for this problem is scaled to the RC time,

$$\Omega \equiv \frac{\varepsilon_w \Lambda L}{\sigma \lambda_D} \omega. \tag{9}$$

Similarly, Eq. (7) dictates that the velocity be scaled to the usual reference value for ICEO flows in the low-voltage model,

$$U_{ref} \equiv \frac{\varepsilon_w \Lambda V_{peak}^2}{\eta L}. \tag{10}$$

All the simulated data is presented and discussed below using these scales. The results of the parametric simulations for pumping velocities using two different step heights as a function of operating frequencies are presented in Fig. 4. As described in the caption of the figure, the theoretical results for the maximum flow rate and peak frequency in the linear model are reasonably close to the corresponding experimental values, if we choose $\Lambda = 0.2$ or $\delta = 4$, which seems consistent with prior estimates of the degree to which the simplest theory (neglecting the compact layer) over-estimates the flow rate [8,17]. The pumping performance for moderate (near optimal) and high
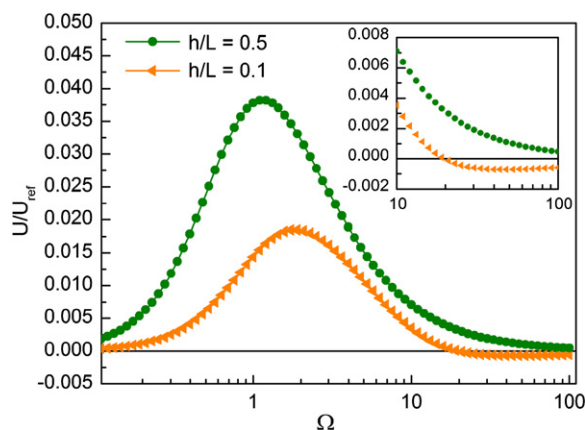
Fig. 4. Performance of pumps consisting of different step heights as a function of driving frequency. For moderate nondimensional driving frequencies ($\Omega \approx 1$), fast flows are developed as a result of the fluid conveyor belt principle. At high operating frequencies, negative pumping velocities, counter to the expected FCB mechanism, are observed for small values of h. The inset clarifies this flow reversal. If we fix $\Lambda = 0.2$ (or $\delta = 4$) for a 3 μM KCL solution, then the peak forward pumping in the figure occurs at 980 Hz. Taking into account hydraulic resistance, an effective pressure head is used to relate the simulated ACEO results to the expected fluid velocity in our microfluidic loop. Using this approach for the present channel and pump geometry, the ratio of the 3D expected centerline velocity to the 2D predicted average velocity is approximately 0.36. For example, if we model the input of $3V_{pp}$ and 980 Hz, the average outlet flow velocity of 1.2 mm/s would correspond to an expected 440 μm/s maximum velocity in the loop. Although 2D simulations neglect resistance of the vertical channel walls, thereby overestimating the generated pressure head, these values obtained from the linear model are reasonably consistent with the experimental data in the figures below.
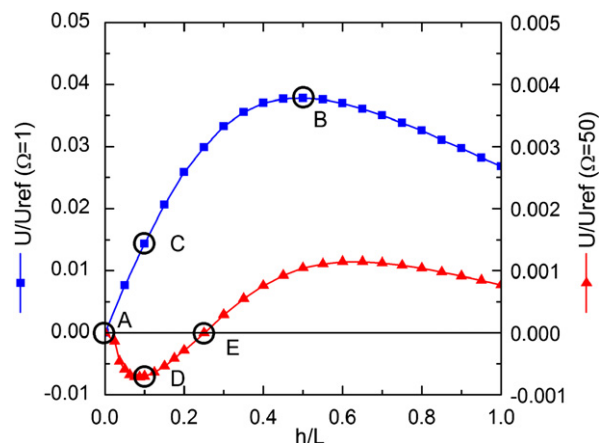

Fig. 5. Average fluid velocity computed across the outlet of the two-dimensional simulation as a function of electrode step height, for a high and low driving frequency. For moderate frequencies ($\Omega \approx 1$), idealized fluid conveyor belt pumping is observed for all h. Fluid streamlines and charging profiles developed in cases A and B are illustrated in Figs. 6A and 6B. At high frequencies ($\Omega > \approx 10$), however, flow reversals are observed for low values of h. In these cases, charges are not able to screen across the entire electrode surfaces, and unexpected flow profiles are developed. At $h/L \approx 0.1$, for example, fluid flow may be switched from positive FCB pumping to reverse flow with a change of driving frequency. The streamlines in cases C and D provide further explanation in Figs. 6C and 6D. Stagnation is also possible at higher frequencies. At point E, the partially developed vortices in the fluid conveyor belt are in balance with the smaller, but raised vortices on the top of the electrode steps. This case is illustrated in Fig. 6E.

(suboptimal) driving frequencies is summarized in Fig. 5 for a range of step heights.

For large step heights, our simulations are consistent with the results of Bazant and Ben [15]. For example, with $h = 0.5L$, the flow rate in Fig. 4 exhibits a single broad peak as a function of frequency consistent with "forward" flow due to the FCB mechanism. The peak frequency is at the expected scale of the characteristic RC charging frequency of the electrode geometry $\Omega \approx 1$. Comparing to their results, the flow rate of the nonplanar 3D ACEO pumps is also much faster than that of standard planar designs with asymmetric flat electrode arrays, by more than an order of magnitude, for the same applied voltage and minimum feature size. Our simulations also support their claim that the fast flow rate is not very sensitive to the precise step height in the FCB regime, as shown in Fig. 5 for $\Omega \approx 1$.

The frequency spectrum for fast pumping with large steps is easily understood in terms of the usual theoretical picture of ACEO flows, illustrated in Figs. 6A and 6B: At low frequencies $\Omega \ll 1$, the double layers have enough time within each AC period to become so charged as to fully screen the electric field, resulting in no electro-osmotic slip; at high frequencies $\Omega \gg 1$, there is not enough time for the double-layers to charge enough to contribute a significant voltage drop to the zeta potential, and hence there is also no slip. The peak at the RC frequency corresponds to a condition where, in each period, the electrode double layers become partially charged near the edges, while leaving the central regions uncharged as sources

of tangential electric field to drive induced electro-osmotic slip over the charged regions.

For smaller step heights, however, we observe a new, more complicated frequency response, albeit at much smaller flow rates. A surprising discovery in our study is that the standard linear model for ACEO flow predicts some degree of flow reversal for nonplanar pumps, which does not occur in planar electrode geometries, even when additional effects are included in the model [10]. As shown in Fig. 5, for $\Omega = 50$, simulations at high frequencies predict reverse flows for small step heights, which are almost as fast as the forward flows resulting from the FCB mechanism for large step heights. The flow reversal clearly indicates a different physical mechanism, although we stress that it only occurs in the linear model at such high frequencies that the flow rate is smaller than the peak by more than an order of magnitude, as shown in Fig. 4 for $h = 0.1L$.

It is instructive to decipher the reason for flow reversal at small step heights in the linear model, since it may also apply to more general nonlinear models, just as the FCB mechanism at large step heights is also likely to be quite robust. In the context of the linear model, the mechanism for flow reversal at small step heights and high frequencies can be understood in terms of nonuniform charging dynamics in the nonplanar electrode geometry, as illustrated in cases C and D of Fig. 7. At moderately high AC frequencies $\Omega \gg 1$, there is only enough time in each period for the double layers to charge close to the edges of the electrodes, where the normal electric field (prior to charging) is largest across the gap between the electrodes. In the nonplanar geometry with asymmetric steps, the edges have different orientations, which affect the tangential electric field

and the slip profile. The edge of the electrode step on the side of the raised surface (on the right of the gap) forms a shielded corner with a small tangential electric field, which reduces the slip compared to the lower electrode surface (on the left). Moreover,
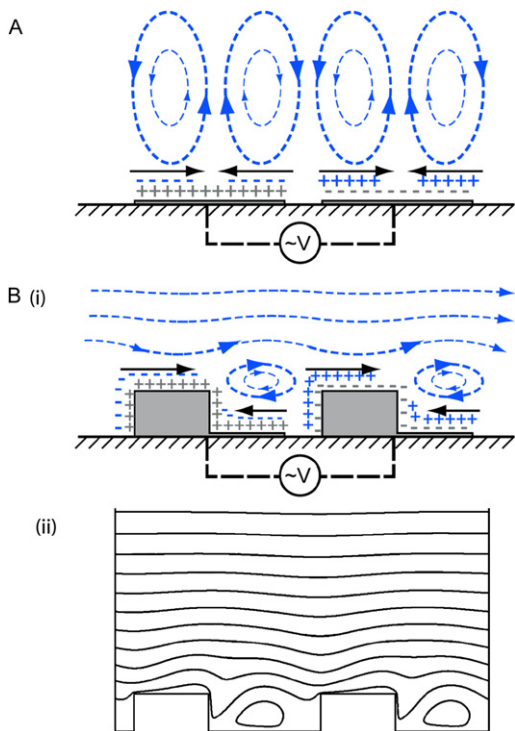

Fig. 6. Schematic illustration of electrohydrodynamic profiles in cases A and B from Fig. 5. Surface slip and time averaged fluid streamlines are represented using solid and dashed arrows, respectively. At moderate frequencies, the double-layer across the entire electrode is allowed to charge, and surface slip is fully developed. (A) If no steps are added to the symmetric electrodes ($h = 0$), complementary vortices are sustained, and no directionality is possible. (B) (i) Charging dynamics are sketched alongside (ii) numerical fluid streamlines. For tall steps ($h \approx 5$ μm), the ideal fluid conveyor belt is developed.

the vertical orientation of the step edge (on the right) leads to slip which cannot pump in either direction, while the edge of the lower electrode surface (on the left) is horizontal and thus efficiently pumps away from the gap.

The net effect is that the lower surface "wins" in pumping in the reverse direction (to the left) for small step heights and high frequencies. At lower frequencies near the optimum, more complete charging occurs across the electrodes, and the vertical edge contribution becomes insignificant, allowing the raised surface to win in pumping in the forward direction (to the right). Naturally, the balance of these two effects leads to an interesting case of zero flow at a special intermediate height and high frequency, in spite of a rather complicated flow profile, as shown in Fig. 7. At large heights, however, edge effects are robustly eliminated at all frequencies, since the FCB mechanism always dominates: For sufficiently raised steps, any reverse flow on the lower surfaces tends to recirculate and help, rather than hinder, the forward flow from the raised surfaces.

4.2. Experimental results

Fluid velocity measurements are performed using a microfluidic device containing dilute KCl with a fixed $3V_{pp}$ operating voltage. A range of driving frequencies from 0.5 to 10 kHz is applied; these are selected only from experience with typical inputs utilized for ACEO pumping and experimental convenience. The experiments are performed with eight different ACEO devices, with step heights in the range of 0 μm (unplated) to 10 μm (plated).

The pumps demonstrate complex velocity-frequency responses with increasing step height. Velocity measurements using a 3 μM KCl concentration are presented in Fig. 8. As expected, there is no directional pumping without the addition of steps. With the addition of sub-micron steps on the electrodes, negative (reverse) pumping is observed at all frequencies. At
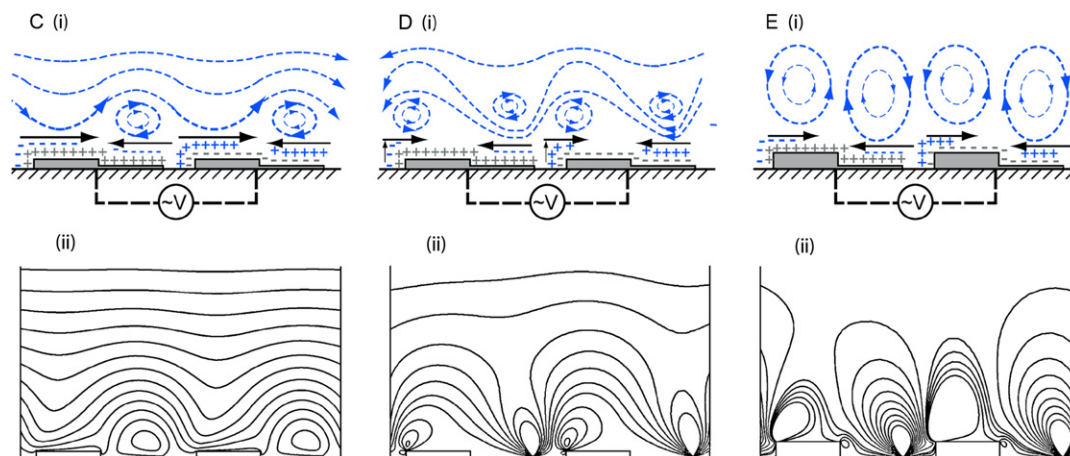

Fig. 7. Schematic illustration of electrohydrodynamic profiles in cases C, D, and E from Fig. 5; (i) charging dynamics are sketched alongside (ii) numerical fluid streamlines. Surface slip and time-averaged fluid streamlines are represented using solid and dashed arrows, respectively. (C) At moderate frequencies, the double layer across the entire electrode is allowed to charge, and FCB pumping can be developed even for low step heights ($h/L \approx 0.1$). (D) For the same h/L, at high frequencies, only portions of the double layer near the strongest fields are allowed to charge. Surface slip on the low electrode portion develops more quickly than that on the step surface due to the geometry. As such, negative pumping is developed counter to the FCB mechanism. (E) An appropriate driving frequency at low step heights can also result in a balance between counter vortices on the nonplanar electrodes. While the surface slip is further developed on the lower electrode surfaces, the smaller vortices are compensated by the step height, and no net pumping is achieved.
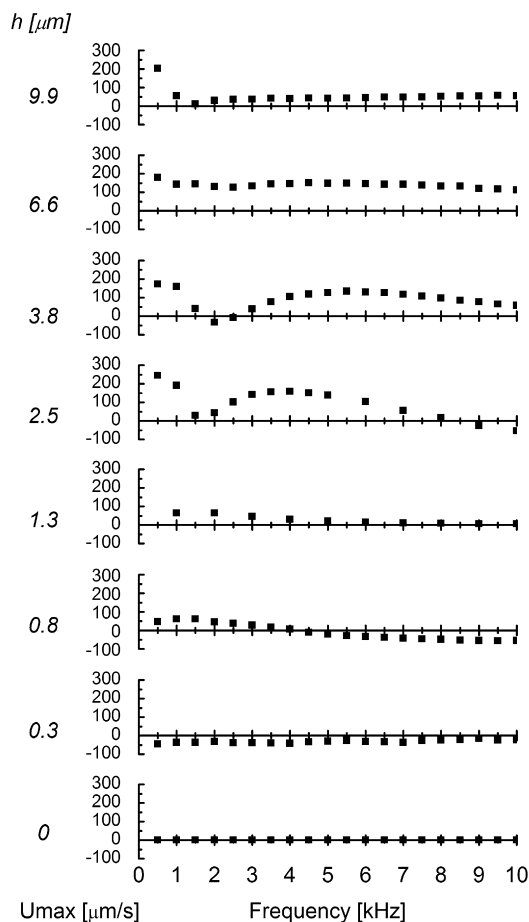
Fig. 8. Centerline fluid velocity measured within microfluidic loops as a function of operating frequency using seven different 3D ACEO pumps. Positive velocity measurements are consistent with the fluid conveyor belt pumping mechanism illustrated in Fig. 1. Negative velocities are also observed for small sub-micron steps. The operating fluid is 3 μM KCl, and pumps are operated at $3V_{pp}$. The "double-peaked" frequency response develops for intermediate step heights, and dampens out as the step height is further increased. At low frequencies, velocity response is difficult to predict, and between pumps of different step heights, peaks do not necessarily align at similar frequencies.

higher plated step heights, the peak velocity—which is attained at lower frequencies—increases to a maximum at a height of around 3.8 μm and decreases up to 9.9 μm. Moreover, a "double peaked" frequency response is evident for intermediate step heights, similar to our previous data for pumping water with other 3D ACEO devices with small step heights [16], although this effect dampens out as the step height is further increased.

The individually-measured velocity-frequency spectrum curves are cross-sectioned to ascertain the effects of electrode step height on the average performance of the nonplanar ACEO pumps. This data is presented in Fig. 9. The "double peaked" response contributes to velocity trends that overlap as h is increased across multiple frequencies. At high frequencies, greater than around 4 kHz, the velocity data as a function of height tends to collapse onto a single curve. A large spread in velocity measurements occurs for intermediate heights ($h \approx$ 2–5 μm), in comparison to pumps with more conservative performance ($h \approx$ 6–10 μm), which suggests interesting design implications.
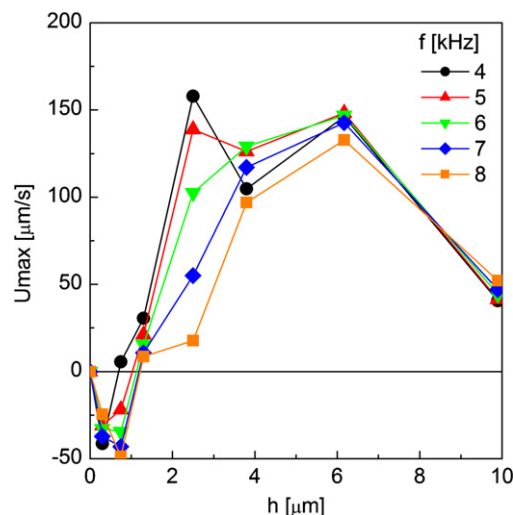

Fig. 9. Centerline fluid velocity as a function of the ACEO electrode step height for various operating frequencies. The fluid is 3 μM KCl, pumped by an AC applied voltage $3V_{pp}$ in the frequency range 4–8 kHz. Following from Fig. 8, peak velocities do not necessarily occur at similar driving frequencies for all pumps, and this frequency shifting results in a range of possible velocities for a given h. At large step heights the flow rate is strong, relatively insensitive to frequency and consistent with the fluid conveyor belt mechanism of Figs. 1B and 6B and the simulations in Fig. 5. The data also shows relatively strong reverse flow at small, sub-micron step heights, which is not predicted by the simple linear model near the peak frequency. The simulations in Fig. 5 do predict a similar trend with height, but only at high frequencies far above the peak, where the flow rate is an order of magnitude smaller.

4.3. Discussion

Several important features are evident in the velocity-frequency response, some of which are more robust than others. At low frequencies, velocity response is sensitive to driving frequency, particularly for pumps with steps in the range of $\approx$2–7 μm. Nonetheless, pumps with step heights in this intermediate range exhibit wide operating ranges, which are less sensitive to frequency, generally above 4 kHz. For low step heights, very fast pumping may be achieved with tuning of the driving frequency; there is a risk, however, of approaching the local minimum operating point (typically falling between 1 and 3 kHz). Taller pumps do not exhibit such behavior, and fast, steady pumping is observed across a wide range of driving frequencies. The tradeoff for a robust operating range is in the decrease of potential pressure head. Such trends should also be expected with different characteristic length scales (combinations of electrode width and gap) and operating voltages.

Pumps with large step heights exhibit robust, positive flow rates, in a direction consistent with the FCB mechanism, but flow reversal is also clearly evident in Fig. 8. The shortest pump ($h = 0.3$ μm) is not capable of pumping in the positive direction within the frequency range tested. Conversely, the taller steps ($h > \approx$6 μm) do not demonstrate flow reversal over the same frequency range. For electrode heights between 0.8 and 2.5 μm, however, transitions between forward and reverse flow occur. Thus systems designed with sufficiently low step heights may be used to pump fluid in both forward and reverse directions by appropriately tuning the driving frequency. This effect could be

exploited to implement potentially useful bi-directional pumps in microfluidic devices. Further, Fig. 8 illustrates that measured peak pumping frequencies differ for systems with increasing step heights. This makes direct comparisons of different pumps difficult at a given operating point, and prior knowledge of this frequency spectrum would be important in the application of newly fabricated devices.

It is worth noting that the experimental details differ somewhat from the simulations. The employed fabrication process uses electroplating to create steps on the planar electrodes. Due to photolithography, however, the steps taper outwards with height as the 10 μm tall photoresist sidewalls are not perfectly vertical. The horizontal surface of the stepped electrodes also exhibit surface roughness due to the nature of electroplating (as observed in Fig. 2a). This is in contrast to the numerical model with straight and perpendicular electrode steps. Alternative photoresist and electroplating chemistries or a more complex microfabrication process could conceivably be used to create more regular geometries in the future, although it remains an open question whether any improvement in device performance warrants the increased complexity.

The minor differences in geometry between the simulations and the experiments, however, are not enough to explain all the discrepancies. Flow rates in both the experiment and in the theory could be affected by uncertainty in the electrolyte concentration tested; however, the standard linear model which we use in our simulations has no dependence on conductivity (concentration) aside from a rescaling of the flow through the Debye length in the parameter Λ (or δ). Comparing the experimental data in Figs. 8 and 9 with the corresponding simulation results in Figs. 5 and 6, respectively, shows that the simple linear model fails to predict some key aspects of the data. The main success of the model is that it captures the dominant FCB mechanism leading to robust and fast forward pumping at large step heights, but it does not properly describe the frequency response at smaller step heights. For example, the simulations in Fig. 5 generally fail to predict the double-peaked frequency response seen experimentally at intermediate step heights in Fig. 8. For small steps, the simulations in Figs. 5 and 6 only exhibit a very weak flow reversal at high frequencies, while the experimental data in Figs. 8 and 9 shows fairly strong reverse flow at the same peak operating frequency as the optimal FCB flow at larger step heights. Nevertheless, we expect that the basic explanation of the flow reversal, involving partial charging at the electrode edges, might also apply to a more accurate nonlinear model (see below).

There are a variety of known shortcomings of the standard model, which are beginning to be addressed. As noted above, the model can only be rigorously justified in the limit of small applied voltages, $V \ll kT/e = 25$ mV [22], which are over 100 times smaller than those used in most ACEO experiments. The classical electrokinetic equations, based on the Poisson–Boltzmann model of the double layer, predict a number of nonlinear effects in this regime, such as increased double-layer differential capacitance [10], neutral salt adsorption and tangential conduction [25,26], and Faradaic reactions may also set in at large voltages [10]. However, it seems that these nonlinear ef-

fects only make the agreement between theory and experiment worse for planar ACEO pumps [10,11]. For example, none of these modifications can predict the high-frequency flow reversal observed in experiments with planar ACEO pumps [9]. We expect that the flow reversal at small step heights in our model would also be difficult to explain with the classical nonlinear model.

In any case, there is clearly a need to develop better models for ACEO flows at the typical large applied voltages used in experiments, and some efforts are already underway [27]. Perhaps the most obvious problem with the Poisson–Boltzmann model of the diffuse layer is that it completely breaks down at large voltages across the diffuse layer, $V \gg kT/e$, by predicting absurd ion concentrations exceeding the close-packing limit. Simple modified equations taking into account steric effects can have major implications for charging dynamics [23,24], which may help explain our experimental data. In particular, the differential capacitance is generally predicted to decrease at large voltages due to steric effects (the opposite trend of Poisson–Boltzmann theory), which would cause the electrode edges to charge faster than the central region due to nonlinearity, without changing the AC frequency. This could explain why the edge effects leading to flow reversal in the linear model at high frequency (Fig. 7) actually occur in the experiments at the much lower peak frequency.

5. Summary

In conclusion, we have furthered the recent advance of 3D ACEO pumping with nonplanar electrodes by experimentally and numerically varying the principal geometrical parameter, the step height, which has profound effects on pump performance.

At large step heights, we have confirmed the qualitative predictions of Bazant and Ben of fast pumping for a broad range of frequencies and step heights by the fluid conveyor belt mechanism [15]. By applying only a few Volts at kHz frequencies, we have demonstrated robust average velocities well over 100 μm/s in a microfluidic loop only 25% covered by the electrode array (for measurement purposes). Therefore, mm/s velocities at the same voltages should be attainable in practical devices more completely covered by pumping surfaces. As demonstrated in our preliminary work, these flows are much faster than with planar ACEO pumps, under similar conditions [16]. The 3D ACEO pumps with tall steps are also more robust than previous planar designs, since they provide reliable, fast pumping for a wide range of geometrical and operating conditions, always in the same direction predicted by the simple FCB mechanism. In contrast, planar pumps suffer flow reversals with varying voltage or frequency, which are not yet understood. This new capability could find many uses lab-on-a-chip technology, especially in portable or implantable devices needing to operate at low power and low voltage, powered by a small battery.

We have also observed some interesting and unexpected departures from the theory of Bazant and Ben in our experiments. The dominant fluid conveyor belt mechanism breaks down for

insufficiently tall step features, and we have suggested a new mechanism leading to flow reversal with small steps (Fig. 7). Our explanation relies on partial charging near the edges of the nonplanar electrodes, which only occurs at high frequencies in the standard low-voltage linear model, but we expect that a similar mechanism may apply at normal operating frequencies in a more accurate nonlinear model, as in the experiments. Comparing our simulations to the experiments, however, shows that, although useful qualitative predictions can be made, important features are clearly missing in the simple linear model. For example, the model cannot explain for the double-peaked frequency response which arises at intermediate step heights in these experiments, as in our preliminary work [16]. As such, our data contributes to the growing body of performance measurements for ACEO pumps, which can serve to guide the development of improved theoretical models for induced-charge electrokinetics at large voltages [27].

Acknowledgments

References

[1] T.M. Squires, S.R. Quake, Rev. Mod. Phys. 77 (3) (2005) 977–1026.
[2] D.J. Laser, J.G. Santiago, J. Micromech. Microeng. 14 (6) (2004) R35–R64.
[3] H. Lin, B.D. Storey, M.H. Oddy, C.H. Chen, J.G. Santiago, Phys. Fluids 16 (6) (2004) 1922–1935.
[4] A. Ramos, H. Morgan, N.G. Green, A. Castellanos, J. Colloid Interface Sci. 217 (2) (1999) 420–422.
[5] A. Ajdari, Phys. Rev. E 61 (1) (2000) R45–R48.
[6] A.B.D. Brown, C.G. Smith, A.R. Rennie, Phys. Rev. E 63 (2) (2001) 016305.
[7] M. Mpholo, C.G. Smith, A.B.D. Brown, Sens. Actuat. B 92 (3) (2003) 262–268.
[8] N.G. Green, A. Ramos, A. Gonzalez, H. Morgan, A. Castellanos, Phys. Rev. E 66 (2) (2002) 026305.
[9] V. Studer, A. Pepin, Y. Chen, A. Ajdari, Analyst 129 (10) (2004) 944–949.
[10] L.H. Olesen, H. Bruus, A. Ajdari, Phys. Rev. E 73 (5) (2006) 056313.
[11] L.H. Olesen, Ph.D. Thesis, Technical University of Denmark, 2006.
[12] A. Ramos, A. Gonzalez, A. Castellanos, N.G. Green, H. Morgan, Phys. Rev. E 67 (5) (2003) 056302.
[13] B.P. Cahill, L.J. Heyderman, J. Gobrecht, A. Stemmer, Phys. Rev. E 70 (3) (2004) 036305.
[14] A. Ramos, H. Morgan, N.G. Green, A. Gonzalez, A. Castellanos, J. Appl. Phys. 97 (8) (2005) 084906.
[15] M.Z. Bazant, Y. Ben, Lab. Chip 6 (11) (2006) 1455–1461.
[16] J.P. Urbanski, T. Thorsen, J.A. Levitan, M.Z. Bazant, Appl. Phys. Lett. 89 (14) (2006) 143508.
[17] J.A. Levitan, S. Devasenathipathy, V. Studer, Y.X. Ben, T. Thorsen, T.M. Squires, M.Z. Bazant, Colloids Surf. A 267 (1–3) (2005) 122–132.
[18] M.A. Unger, H.P. Chou, T. Thorsen, A. Scherer, S.R. Quake, Science 288 (5463) (2000) 113–116.
[19] V. Studer, G. Hang, A. Pandolfi, M. Ortiz, W.F. Anderson, S.R. Quake, J. Appl. Phys. 95 (1) (2004) 393–398.
[20] A. Gonzalez, A. Ramos, N.G. Green, A. Castellanos, H. Morgan, Phys. Rev. E 61 (4) (2000) 4019–4028.
[21] M.Z. Bazant, T.M. Squires, Phys. Rev. Lett. 92 (6) (2004) 066101.
[22] T.M. Squires, M.Z. Bazant, J. Fluid Mech. 509 (2004) 217–252.
[23] M.S. Kilic, M.Z. Bazant, (2006), submitted for publication.
[24] M.S. Kilic, M.Z. Bazant, A. Ajdari, (2006), submitted for publication.
[25] M.Z. Bazant, K. Thornton, A. Ajdari, Phys. Rev. E 70 (2) (2004) 021506.
[26] K.T. Chu, M.Z. Bazant, Phys. Rev. E 74 (1) (2006) 011501.
[27] M.Z. Bazant, M.S. Kilic, B. Storey, A. Ajdari, (2006), submitted for publication.